Data-driven Exponential Framing for Pulsive Temporal Patterns without Repetition or Singularity

Yohei Kono

Chief Researcher Research & Development Group Hitachi, Ltd. Yoshidacho 292, Totsuka, Yokohama, 244-0817 Japan

Email: yohei.kono.un@hitachi.com

Yoshiyuki Tajima

Manager Research & Development Group Hitachi, Ltd. Yoshidacho 292, Totsuka, Yokohama, 244-0817 Japan Email: yoshiyuki.tajima.hh@hitachi.com

Extracting pulsive temporal patterns from a small dataset without their repetition or singularity shows significant importance in manufacturing applications but does not sufficiently attract scientific attention. We propose to quantify how long temporal patterns appear without relying on their repetition or singularity, enabling to extract such temporal patterns from a small dataset. Inspired by the celebrated time delay embedding and data-driven Hankel matrix analysis, we introduce a linear dynamical system model on the time-delay coordinates behind the data to derive the discrete-time bases each of which has a distinct exponential decay constant. The derived bases are fitted onto subsequences that are extracted with a sliding window in order to quantify how long patterns are dominant in the set of subsequences. We call the quantification method Data-driven Exponential Framing (DEF). A toy model-based experiment shows that DEF can identify multiple patterns with distinct lengths. DEF is also applied to electric current measurement on a punching machine, showing its possibility to extract multiple patterns from real-world oscillatory data.

1 INTRODUCTION

Temporal patterns, meaning subsequences which are in some sense representative of their original time-series data, play a crucial role in various research areas [1, 2, 3, 4, 5, 6]. This paper suggests an alternate perspective on continuous-valued temporal patterns that is more suitable for manufacturing applications.

In manufacturing processes, the development of

sensing and information technologies has accelerated data-driven enhancement of their operation and maintenance. This trend motivates the use of temporal patterns for monitoring complex phenomena that cannot be described in closed-form models. For instance, in the case of injection-molding machines, Takatsugi, et al. [7] reported that temporal patterns in load torque data can characterize in-situ resin pressure, and proposed detecting the reverse flow of resin by monitoring the data. Similarly, for punching machines, Takahashi, et al. [8] analyzed a temporal pattern in die acceleration data to monitor the tool wear. For human manufacturing, Terada, et al. [9] developed an unsupervised method for detecting a series of repetitive actions by recognizing basic actions from human motion data. We also developed an anomaly detection method based on temporal patterns and applied it to manufacturing machines [10].

Motivated by the above studies, we address data-driven extraction of temporal patterns specific to manufacturing processes. The time-series data and patterns addressed here are characterized by the three assumptions. Firstly, as in manufacturing machines operated with the position or speed control of their tools (e.g., Ref. [11]) and chemical processes controlled on different levels of temperature reference, reference values (setpoints) for control of manufacturing processes can jump discretely, leading to process data containing rapidly rising (or falling) curves or irregular oscillations. These patterns are referred to as hereafter *pulsive temporal patterns* in this paper. Secondly, the manufacturing process has multiple modes of operation where the frequency of occurrence

of each mode is not necessarily high. This means that the number of occurrence of each temporal pattern can be few in number, including one-shot occurrence. Thirdly, pulsive temporal patterns relevant in engineering practice are not restricted to anomalous events or singular behaviors. Many relevant cases, such as transient responses to external inputs or one-off operational changes, occur without singularities, implying the necessity to develop a framework that can address one-shot patterns, with or without singularity, beyond the conventional scope of anomaly detection. Therefore, this paper aims to extract pulsive temporal patterns from a small dataset that may lack repeated instances.

Research on extracting pulsive temporal patterns has largely been conducted using machine learning techniques, specifically time-series data mining [12]. Different definitions of temporal patterns exist based on the machine learning task at hand. Ref. [13] defined previously unknown, frequently occurring patterns as motifs and developed a discovery algorithm for them. In the last two decades, many research groups have developed sophisticated algorithms for finding motifs [14, 15]. Ref. [16] introduced time series discords, which are subsequences of a longer time series that are maximally different from all the rest, making it highly compatible with anomaly detection; see, e.g., [17, 18]. Ref. [19] addressed the classification problem of time series and formulated a concept of time series shapelet, which are subsequences maximally representative of a class. Jointly learning shapelets and a classifier has also been reported in Refs. [20, 21]. These studies suggest that previous definitions of temporal patterns rely on repetition or singularity.

However, to the best of our knowledge, not enough attention has been given to identifying pulsive patterns in small datasets. This suggests that additional criteria, beyond repetition or singularity, are necessary to characterize temporal patterns.

To quantify how long patterns appear in pulsive time series in an unsupervised manner, we propose an alternative view of the temporal patterns based on their length. Inspired by the celebrated time delay embedding [22, 23, 24] and data-driven Hankel matrix analysis [25, 26, 27], we introduce a linear dynamical system model on the time-delay coordinates behind the data to derive the discrete-time bases, each of which has a distinct exponential decay constant. These bases are then fitted onto subsequences that are extracted with a sliding window to determine how long patterns are dominant in the set of subsequences. We call this quantification method *Data-driven Exponential Framing* (DEF). We demonstrate the effectiveness of DEF using artificial data generated by a toy model based on the harmonic os-

cillator. Our results show that DEF can identify multiple patterns with distinct lengths. In addition, we apply DEF to electric current data measured in a punching machine and show its effectiveness in this real-world scenario. Note that this paper is a joint submission with our conference paper [28], and the discrete-time bases with exponential decay constants have been proposed in our non-archival conference paper [10].

The contributions of this paper are twofold. The first capability is the development of a practical method for characterizing small timeseries datasets. The method extracts dominant temporal patterns from a timeseries dataset without their repetition or singularity, which can be search queries for the timeseries data mining. The second contribution is the construction of an alternate framework for decomposing timeseries based on the exponential decay rate. This DEF framework enables the identification of multiple (complex) frequencies that explain pulsive patterns in timeseries data. In simpler terms, DEF offers an alternative interpretation of the modal components calculated by the Singular Spectrum Analysis [25, 29] or the extensions of Dynamic Mode Decomposition (DMD) [30] to Hankel matrices [26, 27].

The rest of this paper is organized as follows. Sec. 2 focuses on explaining the mathematical concept of DEF and its computation algorithm. In Sec. 3, we provide evidence that DEF can identify the lengths of dominant subsequences in numerical data obtained from a toy model. Additionally, in Sec. 4, we demonstrate that DEF can identify multiple patterns with different lengths that are inherent in time series obtained from a manufacturing machine. Sec. 5 shows comparative analysis with SSA and DMD, which evaluates the novelty of proposed DEF method. Finally, Sec. 6 concludes this paper for future research.

2 PROPOSED METHOD

We begin by formulating a state-space description for a scalar output y(t). Let $x(t) \in \mathbb{R}^n$ and $u(t) \in \mathbb{R}^m$ be the state and exogenous input at time t. The state-space systems are formulated as

$$\frac{\mathrm{d}\boldsymbol{x}}{\mathrm{d}t} = f(\boldsymbol{x}, \boldsymbol{u}),\tag{1}$$

$$y = g(x), \tag{2}$$

where $f: \mathbb{R}^n \times \mathbb{R}^m \to \mathbb{R}^n$ is the map of dynamics and $g: \mathbb{R}^n \to \mathbb{R}$ the observable. We consider Eq. (1) as closed-loop (controlled) systems to represent both the physical properties of manufacturing machines and their

controllers' properties. This means that the u(t) can include reference signals (setpoints) for controlling manufacturing machines as well as control parameters. As in a wide range of industrial machines that have a finite number of operation modes, we assume that the reference signals and control parameters jump only under certain conditions, and otherwise remain constant. Therefore, u(t)can be represented by a piecewise constant PWC function, which is a combination of finite-length step signals. As a result, $\{y(t)\}$ involves rapidly rising (or falling) curves or irregular oscillations near the jump, referred to as pulsive patterns. When exogenous inputs are not PWC, the formulation below extends in a straightforward manner by augmenting the delay vector with a finite number of input-lag terms; we keep the exposition focused on the PWC case for simplicity, and discuss this extension in Appendix A.

2.1 Mathematical idea

We propose a method for quantifying the duration of dominant patterns in a given time series. The approach involves analyzing the decaying components within the time series and estimating them based on the evolution of subsequences. This allows us to better understand the behavior of the time series and identify the most significant patterns that contribute to its overall trend.

In order to analyze the patterns in y(t), we first introduce the dynamical formulation of subsequences. Since our focus is on characterizing patterns included in y(t), we rewrite Eq. (1) as the *piecewise autonomous* system by viewing $\boldsymbol{u}(t)$ as a certain fixed function. We also assume that the state \boldsymbol{x} is kept near its equilibrium by control efforts, which allows us to linearize the nonlinear system $\{f,g\}$. Inspired by the delay embedding techniques (see, e.g., [22]) and their capability of formulating state-space dynamics [31], we consider identifying the target linear dynamics from the data on y(t):

$$\frac{\mathrm{d}\boldsymbol{x}_d}{\mathrm{d}t} = \mathsf{A}_d \boldsymbol{x}_d(t),\tag{3}$$

where $x_d \in \mathbb{R}^d$ is the delay-coordinate vector with the degree d, and written with the sampling period Δt :

$$\boldsymbol{x}_{d}(t) = \begin{bmatrix} y(t) \\ y(t - \Delta t) \\ \vdots \\ y(t - (d-1)\Delta t) \end{bmatrix}. \tag{4}$$

Note that Eq. (3) models the time-evolution of subsequences. We will use this perspective to decompose time

series data by their exponential decay rates.

Let us develop a method for characterizing timescales contained in the subsequences. Assuming that A_d is a full-rank matrix, it can be factorized with d linearly independent eigenvectors $V_1 \cdots V_d \in \mathbb{C}^d$ and the corresponding eigenvalues $\lambda_1, \lambda_2, \ldots, \lambda_d$:

$$A_d = V_d \Lambda_d V_d^{-1}, \tag{5}$$

where $V_d = [V_1 \cdots V_d]$ and Λ_d is the diagonal matrix whose diagonal elements are $\lambda_1, \lambda_2, \dots, \lambda_d$. Note that the V_1, \dots, V_d are equivalent to the modal components calculated by SSA [25] and DMD with the Hankel matrices [26, 27]. Based on this decomposition, we consider predicting x_d from an initial time $t = t_0$. Combining Eq. (3) and Eq. (5), the L-steps ahead prediction of x_d is described as follows:

$$\mathbf{x}_{d}(t_{0} + L\Delta t) = e^{\mathsf{A}_{d}L\Delta t} \mathbf{x}_{d}(t_{0})$$

$$= \mathsf{V}_{d} \begin{bmatrix} e^{\lambda_{1}L\Delta t} \\ & \ddots \\ & e^{\lambda_{d}L\Delta t} \end{bmatrix} \mathsf{V}_{d}^{-1} \mathbf{x}_{d}(t_{0})$$

$$= \sum_{i=1}^{d} a_{i,d}(t_{0}) e^{\lambda_{i}L\Delta t} \mathbf{V}_{i}$$
(6)

where $a_{i,d}(t_0)$ is the i-th component of $V_d^{-1} \boldsymbol{x}_d(t_0) \in \mathbb{C}^d$. Eq. (6) implies that each subsequence evolves with the initial time-dependent coefficients $a_{i,d}(t_0)$ on the space spanned by $\{\boldsymbol{V}_i\}$. Here, we assume that the underlying continuous-time signal y(t) can be represented as a finite linear combination of exponential modes $y(t) = \sum_j \exp(\lambda_j^{\text{true}}t)$, which corresponds to a system with a discrete spectrum $\{\lambda_j^{\text{true}}\}$. This assumption is commonly employed in finite-dimensional linear approximations of nonlinear dynamical systems [32]. Then, each $\boldsymbol{V}_i = [v_{i,1}, \dots, v_{i,d}]$ needs to be a sequence of discrete-time exponential functions:

$$\boldsymbol{V}_{i} \simeq b_{i} \begin{bmatrix} \exp\{\nu_{i}((d-1)\Delta t)\} \\ \exp\{\nu_{i}((d-2)\Delta t)\} \\ \vdots \\ 1 \end{bmatrix}, b_{i}, \nu_{i} \in \mathbb{C}. \quad (7)$$

In contrast to $\exp(\lambda_i t)$, which denotes the map from one subsequence to another, the component $\exp(\nu_i t)$ measures *transient* responses contained in each subsequence.

Thus, the real part of $\exp(\nu_i t)$ corresponds to the decaying rate of the responses. We propose the perspective that the decaying rate indicates the lengths (or timescales) of temporal patterns. By combining Eq. (6) and (7) and by setting L=0, we approximate original y(t) by superposing the components $\exp(\nu_i t)^1$: for $n=0,1,\ldots,d-1$,

$$y(t - n\Delta t) \simeq \sum_{i=1}^{d} a_{i,d}(t) \exp\left(\nu_i (d - n - 1)\Delta t\right)$$
$$= \sum_{i=1}^{d} \tilde{a}_{i,d}(t) \exp\left(-\nu_i n\Delta t\right), \tag{8}$$

where t_0 is rewritten by t, and the coefficient $\tilde{a}_{i,d}(t) := a_{i,d}(t) \exp\{\nu_i(d-1)\Delta t\}$ indicates how the component with ν_i is dominant in the interval $[t-d\Delta t,t]$. Assuming each ν_i is distinct so that $\{\exp(\nu_i t)\}$ are linearly independent functions on $[t-d\Delta t,t]$, we propose to estimate $\tilde{a}_{i,d}(t)$ by projecting y(t) onto $\exp(\nu_i t)$:

$$\tilde{a}_{i,d}(t) \simeq \sum_{n=0}^{d-1} y(t - n\Delta t) \exp(\nu_i n\Delta t) =: \tilde{A}_{i,d}(t). \quad (9)$$

The $\tilde{A}_{i,d}(t)$ helps to find dominant transient responses on $[t-d\Delta t,t]$. Below, by representing $\nu_i=\sigma_i+\mathrm{i}\omega_i$ ($\sigma_i\in\mathbb{R}$ and $\omega_i\in[0,2\pi]$), we introduce the i-th time constant $T_i:=1/\sigma_i$ as the timescale of the pattern that appears on $[t_0-d\Delta t,t_0]$ and involves $\tilde{A}_{i,d}(t)$.

2.2 Implementation

We have developed an algorithm to characterize lengths of temporal patterns based on the idea mentioned above. The challenge now is to determine an appropriate value for d, which represents the degree of the delay coordinates. In terms of extracting temporal patterns, d should be greater than the length of the longest pattern of interest. However, a large value of d should be avoided as it can lead to overfitting of A_d , which can negatively impact the extraction of essential dynamic properties. To address this challenge, we suggest using the Akaike Information Criterion (AIC; see Refs. [33, 34]) to determine the appropriate value of d.

Let us prepare mathematical formulations for identifying A_d and determining d. Consider the discrete-time data y[n] (n = 0, 1, ..., N - 1) sampled from the continuous time series y(t) and its delay coordinate vector

 $m{x}_d[n] = [y[n], y[n-1], \dots, y[n-d+1]]^{ op}$. We introduce the data matrices $\mathbf{X}_d^{(M_1,M_2)}, \mathbf{Y}_d^{(M_1,M_2)} \in \mathbb{R}^{d \times (M_2-M_1)}$, denoted by

$$\mathsf{X}_{d}^{(M_{1},M_{2})} = \left[\boldsymbol{x}_{d}[M_{1}-1], \dots, \boldsymbol{x}_{d}[M_{2}-2] \right], \quad (10)$$

$$\mathsf{Y}_d^{(M_1,M_2)} = [\boldsymbol{x}_d[M_1], \dots, \boldsymbol{x}_d[M_2 - 1]],$$
 (11)

where each sample $x_d[n]$ is stacked as a column vector, so that $\mathsf{X}_d^{(M_1,M_2)}$ and $\mathsf{Y}_d^{(M_1,M_2)}$ are matrices of size (state dimension \times number of samples). Given a certain degree d, A_d is derived as a temporally discretized form $\tilde{\mathsf{A}}_d$ by minimizing the following 1-ahead prediction error:

$$E_d = \left\| \mathsf{Y}_d^{(d,N)} - \tilde{\mathsf{A}}_d \mathsf{X}_d^{(d,N)} \right\|_{\mathsf{F}}^2, \tag{12}$$

where $\|\cdot\|_{\mathrm{F}}$ denotes the Frobenius norm. The minimization of the cost function (12) with respect to $\tilde{\mathsf{A}}_d$ reduces to a standard least-squares problem. Specifically, solving

$$\tilde{\mathsf{A}}_d \left(\mathsf{X}_d^{(d,N)} (\mathsf{X}_d^{(d,N)})^\top \right) = \mathsf{Y}_d^{(d,N)} (\mathsf{X}_d^{(d,N)})^\top, \quad (13)$$

yields the closed-form solution

$$\tilde{\mathsf{A}}_{d} = \mathsf{Y}_{d}^{(d,N)}(\mathsf{X}_{d}^{(d,N)})^{\top} \left(\mathsf{X}_{d}^{(d,N)}(\mathsf{X}_{d}^{(d,N)})^{\top}\right)^{-1}. \tag{14}$$

This corresponds to the ordinary least-squares estimator². However, it is necessary to regularize Eq. (12) to avoid the overfitting of \tilde{A}_d to the training dataset $\{X_d, Y_d\}$. We use the prediction horizon L larger than 1 to generate a test dataset different from $\{X_d, Y_d\}$ and introduce the AIC, which is the relative quality of statistical models for a given dataset. Under a fixed L > 1, the AIC for the L-ahead linear regression model is given by

$$AIC(d) = \frac{\left\| \mathsf{Y}_{d}^{(d+L-1,N)} - \mathsf{C}_{d} \tilde{\mathsf{A}}_{d}^{L} \mathsf{X}_{d}^{(d,N-L+1)} \right\|_{\mathrm{F}}^{2}}{N - d - L} + \frac{2d}{N - d - L} \sigma^{2}, \tag{15}$$

¹While we present the formulation for scalar outputs for clarity, the scheme naturally extends to vector-valued outputs by applying the same construction element-wise.

 $^{^2}$ In the present study, no additional regularization (e.g., L1 or L2 penalty) was imposed, since the datasets considered here allowed for a stable estimation. Nevertheless, regularization could be incorporated into Eq. (12) in future extensions to improve robustness when $X_d^{(d,N)}$ is ill-conditioned.

Algorithm 1: Estimation of temporal patterns with optimal delay order d^*

```
Input: Discrete-time samples y[n], candidate set
              \Omega of d, prediction horizon L > 1
   Output: Eigenvalues \{\tilde{\nu}_i\}, amplitudes
                \{\tilde{A}_{i,d^*}[n]\}, and time constants \{\tilde{T}_i\}
1 for d \in \Omega do
         Identify \hat{A}_d by solving the least-squares
          problem in Eq. (12);
        Compute AIC(d) using Eq. (15);
4 Select d^* = \arg\min_{d \in \Omega} AIC(d);
5 Obtain eigenvectors \{\tilde{V}_i\}_{i=1,\dots,d^*} of \tilde{A}_{d^*};
6 for i=1 to d^* do
        Fit a discrete-time exponential curve
           \left[\exp(\tilde{\nu}_i(d-1)), \exp(\tilde{\nu}_i(d-2)), \dots, 1\right] to
          \tilde{\boldsymbol{V}}_i to estimate \tilde{\nu}_i;
        Compute time constant \tilde{T}_i = 1/\text{Re}[\tilde{\nu}_i];
8
         for each time index n do
              Calculate amplitude
10
                \tilde{A}_{i,d^*}[n] = \boldsymbol{x}_{d^*}[n]^{\top} \tilde{\boldsymbol{V}}_i;
```

where $C_d = \widehat{[1,0,\ldots,0]}$ and σ^2 represents the estimate of noise variance. The σ^2 is estimated by signal analvsis or tuned as a regularization parameter. The design parameter L represents the prediction horizon in the information criterion. In principle, there is no universally optimal choice of L. However, its selection significantly affects the behavior of (15). A too small L (e.g., L=1) trivializes the criterion because the prediction horizon is too short, whereas too large L (e.g., $L \ge 10$) tends to destabilize the evaluation due to error accumulation in long-term prediction. In our experiments, we empirically observed that L=5 provides a reasonable trade-off between stability, predictive capability, and the convexity of the information criterion. Therefore, throughout this paper, we fixed L=5 for all experiments. A comparison of different values of L (e.g., L = 1, 5, 10) is provided in Appendix B to illustrate this trade-off.

Based on the formulations, we develop the Algorithm 1 to characterize timescales of temporal patterns inside subsequences. In practice, the dominant peaks were initially identified heuristically, by balancing peak height and spectral isolation from continuous components. This procedure was sufficient to highlight the main temporal scales in the experiments below, but it inherently involves a degree of subjectivity. To improve reproducibility and clarity, we further provide a formalized selection algo-

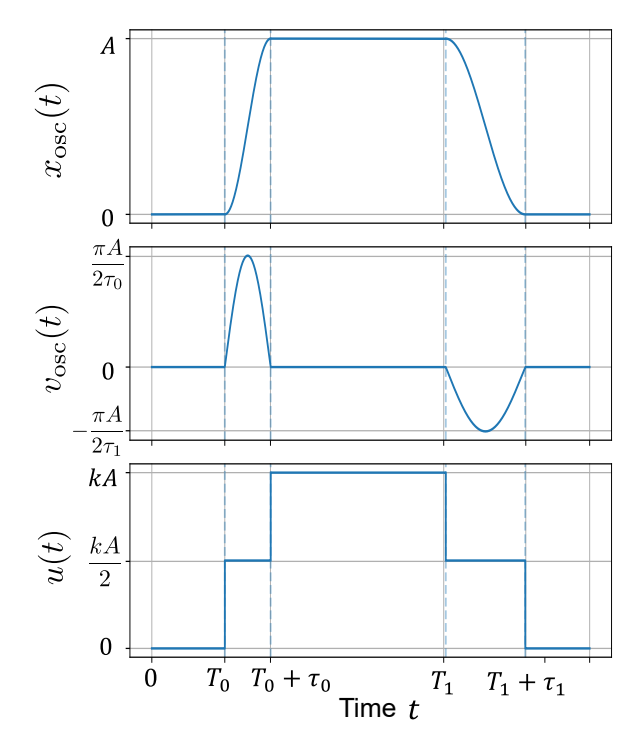


Fig. 1. Trajectory of x(t) and v(t) in Eq. (16) driven by the PWC input u(t).

rithm (Algorithm 2 in Appendix C) that reproduces the same peak candidates in a systematic manner.

Finally, we note how the DEF quantities are used downstream: the triplets $\{(\tilde{\nu}_i, \tilde{V}_i, \tilde{A}_{i,d^*}[n])\}$ act as pattern-level descriptors that bridge raw signals and subsequent analysis/design. They summarize dominant temporal scales per subsequence, enable search/indexing across runs, and provide compact targets for validating or refining physics-based models and controller settings.

3 NUMERICAL VERIFICATION WITH TOY MODEL

In this section, we verify that the proposed method identifies two temporal patterns with their different lengths in numerical data derived from a toy model. As a fundamental model of industrial mechanical systems, we consider a simple harmonic oscillator driven by a piecewise constant (PWC) force u(t) and a switching mass m(t):

$$\frac{\mathrm{d}}{\mathrm{d}t} \begin{bmatrix} x_{\mathrm{osc}}(t) \\ v_{\mathrm{osc}}(t) \end{bmatrix} = \begin{bmatrix} 0 & 1 \\ -\frac{k}{m(t)} & 0 \end{bmatrix} \begin{bmatrix} x_{\mathrm{osc}}(t) \\ v_{\mathrm{osc}}(t) \end{bmatrix} + \begin{bmatrix} 0 \\ \frac{u(t)}{m(t)} \end{bmatrix},$$
(16)

where $x_{\rm osc}(t)$ is the oscillator's position, $v_{\rm osc}(t)$ is the velocity, k is the spring constant. We set the initial condition $x_{\rm osc}(0) = v_{\rm osc}(0) = 0$.

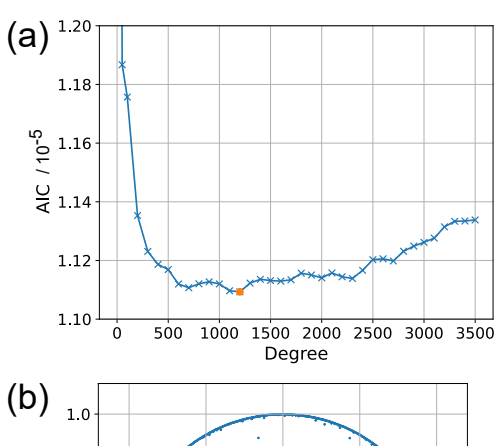
Next, we model the mass m(t) as a PWC function switching between m_0 and m_1 . This switching governs the oscillation timescales: $\tau_0 := \pi \sqrt{m_0/k}$ and $\tau_1 := \pi \sqrt{m_1/k}$ denote the half periods governing the rise and fall segments, respectively. By allowing m(t) to change, the system exhibits trajectories with multiple characteristic frequencies.

On this basis, we introduce the external force u(t) as a designed PWC input. Specifically, u(t) switches through five levels $0 \to \frac{kA}{2} \to kA \to \frac{kA}{2} \to 0$ so that the rise and fall segments each span one half natural period of the oscillator, yielding a half-sine rise to $x_{\rm osc} = A$, a flat plateau at A, and a half-sine return to 0. The schedule is

$$u(t) = \begin{cases} 0, & t < T_0, \\ \frac{kA}{2}, & T_0 \le t < T_0 + \tau_0, \\ kA, & T_0 + \tau_1 \le t < T_1, \\ \frac{kA}{2}, & T_1 \le t < T_1 + \tau_1, \\ 0, & t \ge T_1 + \tau_1, \end{cases}$$
(17)

where $\tau_0 := \pi \sqrt{m_0/k}$ and $\tau_1 := \pi \sqrt{m_1/k}$ denote the half periods for the rise and fall segments (using the corresponding mass values). This PWC excitation u(t) displaces the oscillator from the trivial equilibrium, producing piecewise sinusoidal responses: the trajectory of x(t) consists of a half-sine rise to A, a constant plateau at A, and a half-sine decay to 0. Thus, this section considers a two-input system, (u(t), m(t)). Figure 1 illustrates $x_{\rm osc}(t)$ and $v_{\rm osc}(t)$. Below, we treat $x_{\rm osc}(t)$ as the target time series y(t) analyzed by DEF.

The method for verifying that the DEF can characterize temporal patterns is delineated below. We set A=1, $\tau_0=1000$, $\tau_1=100$, N=15000, $T_0=5000$, and $T_1=10000$ and generate a dataset $\{y[0],\ldots,y[N-1]\}$ with the sampling period $\Delta t=1$. Also, we added the Gaussian noise with its variance of 10^{-6} to the generated data. We applied DEF to the data to compute the time constant \tilde{T}_i and the associated $\tilde{A}_{i,d}[n]$, where σ^2 in Eq. (15) is set at 5×10^{-6} as it is of the same order as the variance of the noise added above. The fitting onto \tilde{V}_i was conducted by <code>scipy.signal.find.peaks</code> in Python. Then, we extract the time constant \tilde{T}_i associated with large $\tilde{A}_{i,d}[n]$ and investigate its validity in comparison with the τ_0 or τ_1 . Note that our method does not



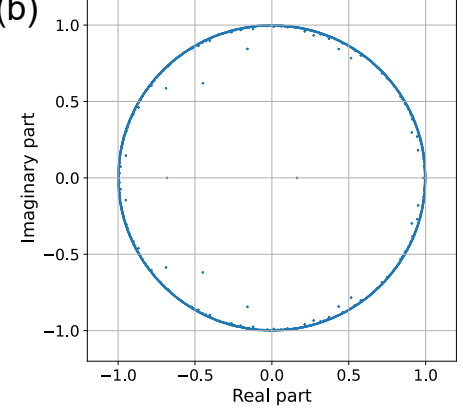


Fig. 2. Preliminary results for the toy model data: (a) Degree d vs. AIC(d), where the orange circle denotes the optimal value d^* , and (b) Eigenvalues of $\tilde{\mathsf{A}}_d$ with d=1200.

impose a strict requirement on the sampling period Δt or the number of samples N. However, as in general signal processing, if Δt is chosen too large relative to the characteristic timescales of the dynamics, the temporal patterns cannot be resolved and extraction becomes difficult. In practice, it suffices to set Δt small enough to resolve these timescales. In our experiments, we selected $\Delta t = 1$ and $\tau_0 = 1000$ (or $\tau_1 = 100$), which were adequate to capture both oscillatory and decay behaviors.

Let us show the preliminary results. Figure 2 (a) shows the AIC values for each degree d, which were set at $\{100, 200, ..., 2000\}$. As d increased, the AIC values decreased and reached their minimum at d=1200. This value of d is close to the length of the first sinusoidal curve ($\tau_0=1000$), which is the longest temporal pattern in the data. Therefore, we adopted d=1200 to characterize the temporal patterns in the rest of this section. Also, Fig. 2 (b) shows the eigenvalues $\{\tilde{\lambda}_i\}$ of \tilde{A}_d computed with d=1200. The $\tilde{\lambda}_i$ lie close to the unit circle, where the distance between any pair of eigenvalues took its minimum of 3.52×10^{-4} . This implies that all the

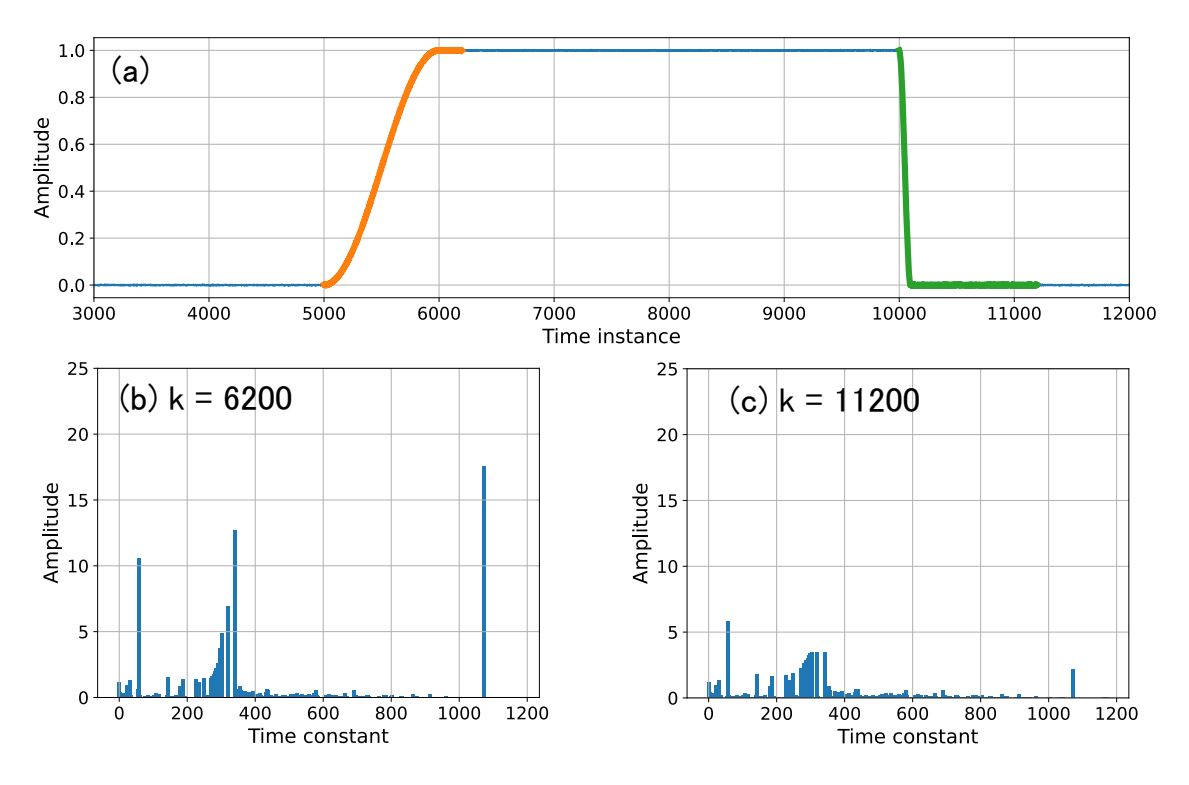


Fig. 3. Main results for the toy model data: (a) The target subsequences $x_{1200}[6200]$ and $x_{1200}[11200]$ highlighted by the bold orange and green lines, respectively. (b,c) The magnitude $\tilde{A}_{i,d}[n]$ at each time constant \tilde{T}_i for (b) n=6200 and (c) n=11200.

 $\tilde{\lambda}_i$ are distinct so that \tilde{A}_d is factorized with d linearly independent eigenvectors, which is the assumption we hold above.

Then, we show the main results of DEF. We focused on the two subsequences $x_{1200}[6200]$ and $x_{1200}[11200]$ that contained the sinusoidal curves highlighted by bold orange and green lines in Fig. 3 (a). The panels (b) and (c) show the magnitude $A_{i,d}[n]$ at each time constant T_i for n = 6200 and n = 11200, respectively. The graph in panel (b) indicates that the amplitude reaches its highest peak at $T_i = 1072.9418$, which suggests that DEF identifies the first sinusoidal curve with its length $\tau_0 = 1000$. Similarly, panel (c) shows that the amplitude takes the highest peak at $\tilde{T}_i = 75.3143$, which is close to the length $\tau_1 = 100$ of the second sinusoidal curve. Here, in both panels (b,c), the amplitude takes large values around $\tilde{T}_i = 341.0002$, but no clear peak appears around this time constant. This finding implies that the exponential components with time constants close to $\tilde{T}_i = 341.0002$ reflect residual content not associated with a single dominant timescale.

Note that the estimation accuracy depends on how the delay order d is aligned with the time scale of the underlying temporal pattern. In the above results with

d=1200, the estimation error for the long-scale pattern ($\tilde{T}_i=1072.94~{\rm vs.}~\tau_0=1000$) is relatively smaller than that for the short-scale pattern ($\tilde{T}_i=75.31~{\rm vs.}~\tau_1=100$). This indicates that shorter windows d are preferable for short-scale patterns, while longer windows are more suitable for long-scale patterns. In practice, one can first apply the method with a broad range $[d_{\rm min}, d_{\rm max}]$ to capture the main peaks, and then re-run the estimation with a restricted window length range around the identified scale to refine accuracy. This two-step strategy was found to be sufficient for engineering use cases.

From the above results and discussion, DEF can quantify how long sinusoidal curves are dominant at each time instance.

4 DEMONSTRATION WITH INDUSTRIAL DATA

This section provides a demonstration of how DEF can extract multiple patterns of different lengths from complex time series data obtained from a manufacturing machine.

The demonstration focuses on a turret punch, which is a type of punch press used for metal forming. Figure 4 shows a schematic diagram of the target turret punch.

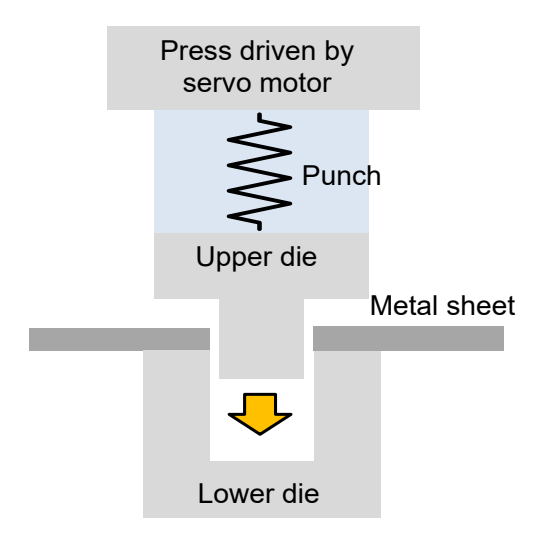


Fig. 4. Schematic diagram of turret punch blanking a metal sheet.

The press is driven by a servo motor and punches an upper die to pierce sheet metal. We collected data on the electric current of the servo motor while driving the press. Figure 5 shows the current data, with 2000 data points, where a metal sheet was punched at n = 830. During the punching process, the reference signal for controlling the vertical position of the upper die jumped to accelerate it, causing intermittent current fluctuations as shown in the figure. Using the reference signal as the input u(t)in Eq. (1), the current data can be naturally described as y(t) generated by Eq. (1) and Eq. (2). As shown in the figure, the representative locations of the data are denoted by L0, L1, ..., L8 to characterize the fluctuation. We verify the possibility of DEF to identify temporal patterns determined by these locations of the data. Note that the setting of DEF was as in Sec. 3; σ^2 was set at 10^{-3} in the same order as the measurement noise, and the fitting onto $\hat{m{V}}_i$ was conducted by scipy.signal.find_peaks.

Let us show the preliminary results for DEF. Figure 6(a) shows the AIC for each d. The AIC took its minimum at d=980, corresponding to the duration while the fluctuation occurred. Therefore, we adopted d=980 to conduct the DEF analysis. Also, 6(b) shows the eigenvalues $\tilde{\mathbf{A}}_d$ for d=980, where the eigenvalues are uniformly distributed around the unit circle and the distance between any pair of eigenvalues took its minimum 1.35972×10^{-3} . Thus, as in the Sec. 3, $\tilde{\mathbf{A}}_d$ is factorized with d linearly independent eigenvectors.

Figure 7 (a) shows the magnitude $\tilde{A}_{i,d}[n]$ at each time constant \tilde{T}_i ($i=1,2,\ldots,d$) for n=1800. The distribution of the $\tilde{A}_{i,d}[n]$ has a finite number of peaks,

implying that DEF can extract dominant bases from the d (= 980) original bases. We address the six peaks called P1-P5 in the panel (a), whose time constants are 36.85, 191.1, 323.8, 492.9, and 600.3, respectively. The time constant for each peak is close to the length of different temporal patterns included in the current data; e.g., the time constant 600.3 of P5 is almost equal to the distance between L0 and L8. To clearly show this, we compute pattern lengths $L_{i,j}$ directly from the real turret punch dataset, defined as the empirical distance between location Li and Lj (e.g., $L_{0,1}$ denotes the distance between L0 and L1). We displayed them separately for their nearest time constant in Fig. 7 (b). The pattern length can be approximated as a linear function of the time constant with its slope of 0.98, implying that the derived time constant represents the length of patterns inherent in the turret punch data. Note that the approximation line deviates from the pattern lengths for P1. Recalling $T_i = 36.85$ for P1 is of a smaller order than d = 980, the deviation implies that DEF is suitable to the identification of an overall (long-term) trend in a subsequence compared to a shortterm one.

From the above results, we contend that DEF can characterize multiple patterns with different lengths.

5 COMPARATIVE ANALYSIS

In order to evaluate the effectiveness of the proposed DEF method, we compare its performance with two widely used decomposition techniques: Singular Spectrum Analysis (SSA) and delay-embedded Dynamic Mode Decomposition (Delay-DMD). For each method, both the toy model data in Sec. 3 and the turret punch data in Sec. 4 are analyzed.

Note that conventional time-series data mining approaches such as motifs [13, 14], discords [16, 17], and shapelets [19, 21] essentially rely on repetition or singularity. These criteria are ill-suited to the present problem setting, where only a limited number of one-shot pulsive patterns are available. In contrast, SSA [25, 29] and DMD [26, 27, 30] share a common reliance on Hankel (trajectory) matrices constructed directly from the observed signal, and thus do not require multiple instances of the same pattern. Accordingly, we adopt SSA and a delayembedded variant of DMD as Hankel-based baselines and compare the time scales they extract against those of DEF. For fairness, the embedding dimension in SSA and Delay-DMD is fixed equal to the DEF delay order d^* (note that d^* differs between the toy system and the turret dataset).

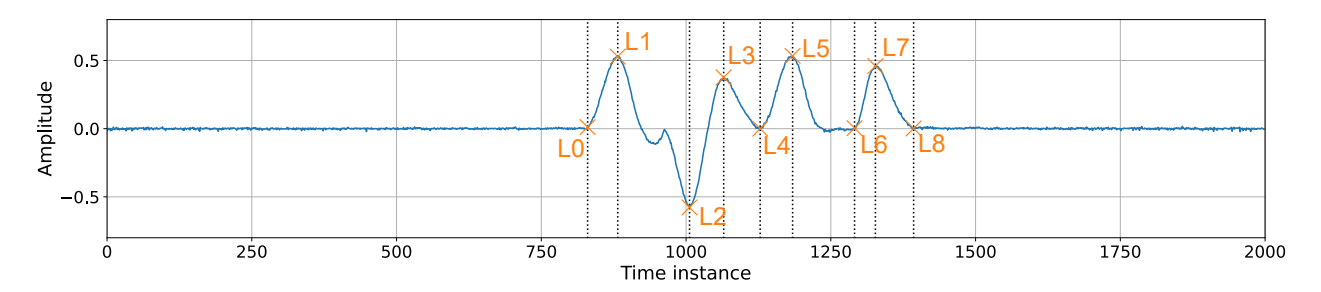


Fig. 5. Target current data measured in the servo motor that drives the press, where the representative locations are denoted by L0, L1, ..., L8.

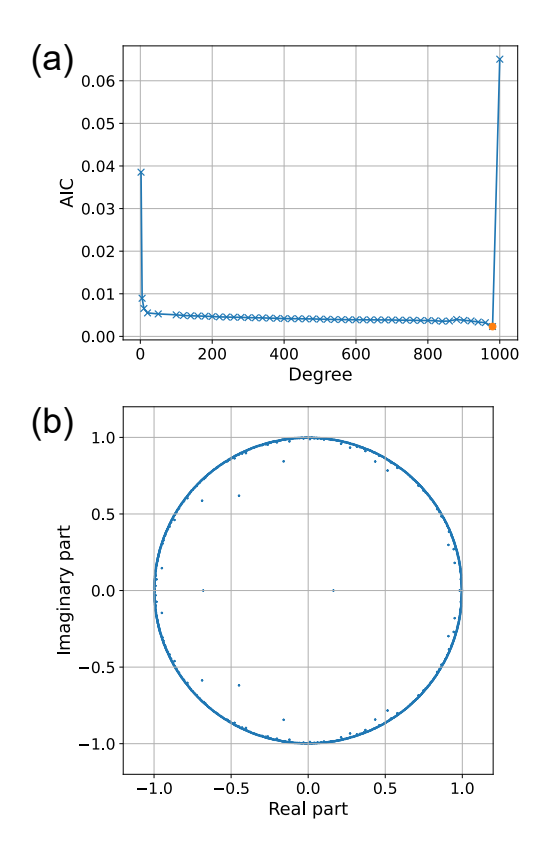


Fig. 6. Preliminary results for the turret punch data: (a) The degree d vs. $\mathrm{AIC}(d)$, where the orange circle denotes the optimal value d^* , and (b) Eigenvalues of $\tilde{\mathsf{A}}_d$ with d=980.

Fig. 7. DEF results for the turret punch: (a) magnitude $\tilde{A}_{i,d}[n]$ for each time constant T_i at n=1800 and (b) pattern lengths $L_{i,j}$ $(i,j\in\{0,\dots,8\})$ computed from the turret punch data, which are separately plotted for their nearest time constant that corresponds to the peaks P1 to P5.

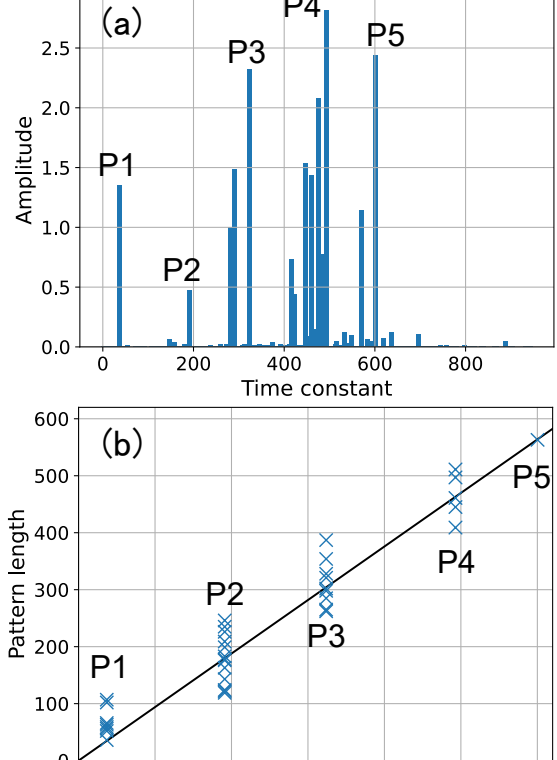
5.1 Baselines via Hankel-structured methods

5.1.1 Singular Spectrum Analysis (SSA)

Let y[n] (n = 0, 1, ..., N - 1) be the discrete-time signal sampled from y(t) with sampling period Δt . Given a window length d (here set to $d = d^*$ to match DEF), we

construct the Hankel (trajectory) matrix

$$\mathbf{X}_{\text{SSA}} = \begin{bmatrix} y[0] & y[1] & \cdots & y[K-1] \\ y[1] & y[2] & \cdots & y[K] \\ \vdots & \vdots & \ddots & \vdots \\ y[d-1] & y[d] & \cdots & y[N-1] \end{bmatrix}, \quad (18)$$



where K := N - d + 1. Applying the SVD to \mathbf{X}_{SSA} ,

$$\mathbf{X}_{\text{SSA}} = \sum_{i=1}^{d} \sigma_i^{\text{SSA}} \, \mathbf{u}_i^{\text{SSA}} (\mathbf{v}_i^{\text{SSA}})^{\mathsf{T}}, \qquad (19)$$

yields singular triplets $(\sigma_i^{\rm SSA}, \mathbf{u}_i^{\rm SSA}, \mathbf{v}_i^{\rm SSA})$. Following standard SSA, reconstructed components (RCs) are obtained by diagonal averaging of selected outer products $\sigma_i^{\rm SSA} \mathbf{u}_i^{\rm SSA} (\mathbf{v}_i^{\rm SSA})^{\rm T}$. We denote the resulting one-dimensional RC signals by $\{\mathrm{RC}_i[n]\}_{i=1}^d$. Since SSA has no unified, principled method to identify the time scale of each $\mathrm{RC}_i[n]$, we qualitatively test the applicability of SSA to identify pattern length in the toy model data and the turret punch data by showing $\mathrm{RC}_1[n]$ and $\mathrm{RC}_2[n]$ as representative waveforms.

5.1.2 Delay-embedded DMD (Delay-DMD)

We apply DMD to the delay-embedded snapshots built from y[n] with the same embedding length $d=d^*$ as DEF. Following the standard (projected) DMD pipeline, we compute a rank-r truncated SVD of $\mathsf{X}_d^{(d,N)}$,

$$\mathsf{X}_{d}^{(d,N)} \approx \mathsf{U}_{r}^{\mathrm{DMD}} \Sigma_{r} (\mathsf{V}_{r}^{\mathrm{DMD}})^{\mathsf{T}},$$
 (20)

and estimate the reduced operator

$$\mathsf{A}^{\mathrm{DMD}} = (\mathsf{U}_r^{\mathrm{DMD}})^{\mathsf{T}} \mathsf{Y}_d^{(d,N)} \mathsf{V}_r^{\mathrm{DMD}} \Sigma_r^{-1}. \tag{21}$$

Let $\mathsf{A}^{\mathrm{DMD}}\mathsf{W} = \mathsf{W}\Lambda$ be its eigendecomposition with $\Lambda = \mathrm{diag}(\lambda_1^{\mathrm{DMD}},\dots,\lambda_r^{\mathrm{DMD}})$ and $\mathsf{W} = [\boldsymbol{w}_1,\dots,\boldsymbol{w}_r]$. The DMD modes in the data space are

$$\Phi = \mathsf{Y}_d^{(d,N)} \mathsf{V}_r^{\mathrm{DMD}} \Sigma_r^{-1} \mathsf{W} = [\phi_1, \dots, \phi_r].$$
 (22)

Continuous-time exponents are obtained by

$$\nu_i^{\text{DMD}} = \frac{1}{\Lambda t} \log \left(\lambda_i^{\text{DMD}} \right) = \alpha_i^{\text{DMD}} + j \omega_i^{\text{DMD}}, (23)$$

and the associated period is

$$T_i^{\mathrm{DMD}} = \frac{2\pi}{|\omega_i^{\mathrm{DMD}}|}, \quad \text{if } \omega_i^{\mathrm{DMD}} \neq 0.$$
 (24)

The quantity T_i^{DMD} indicates the characteristic time scale of (possibly oscillatory) temporal patterns in y[n].

When visualizing T_i^{DMD} , we omit strictly non-oscillatory modes with $|\omega_i^{\text{DMD}}| = 0$.

To quantify the dominance of each DMD mode, we evaluate its global projection contribution over the Hankel snapshots. For the *i*-th DMD mode $\phi_i \in \mathbb{C}^{d^*}$, the orthogonal projector onto $\operatorname{span}\{\phi_i\}$ is

$$\mathsf{P}_i := \frac{\phi_i \, \phi_i^{\mathsf{H}}}{\phi_i^{\mathsf{H}} \phi_i} \in \mathbb{C}^{d^* \times d^*}, \tag{25}$$

where H denotes the Hermitian transpose. Applying P_i to the snapshot matrix yields the portion explained by the i-th mode:

$$\mathsf{X}_{i}^{\mathrm{proj}} := \mathsf{P}_{i} \mathsf{X}_{d}^{(d,N)} \in \mathbb{C}^{d^{*} \times (N-d^{*})}. \tag{26}$$

We define the (global) contribution ratio of mode i by the Frobenius-norm energy ratio

$$c_i^{\text{DMD}} := \frac{\|\mathsf{X}_i^{\text{proj}}\|_{\text{F}}^2}{\|\mathsf{X}_d^{(d,N)}\|_{\text{F}}^2} = \frac{\|\mathsf{P}_i \mathsf{X}_d^{(d,N)}\|_{\text{F}}^2}{\|\mathsf{X}_d^{(d,N)}\|_{\text{F}}^2}.$$
 (27)

In the following, we visualize $T_i^{\rm DMD}$ versus $c_i^{\rm DMD}$ to interpret the time scales of dominant patterns extracted by Delay-DMD.

5.2 Baseline results

5.2.1 SSA

The decomposed waveforms obtained by SSA are shown in Fig. 8(a) for the toy model and Fig. 8(b) for the turret punch data, where the blue and orange lines show reconstructed signals $RC_1[n]$ and $RC_2[n]$, respectively, and the dashed green line shows the input data (toy model or turret punch). For Fig. 8(a), SSA largely reproduces the original input in the leading $RC_1[n]$ and fails to produce a clean separation into distinct pulsive subpatterns. The second component $RC_2[n]$ contains isolated sinusoidal segments that do not correspond to the designed pulsive structure. For Fig. 8(b), both $RC_1[n]$ and $RC_2[n]$ indicate nearly steady sinusoidal curves, so that the transient patterns in the original input are not represented. Thus, in both cases, SSA does not separate the original signal into interpretable pulsive components.

5.2.2 Delay-DMD

The period $T_i^{\rm DMD}$ versus contribution ratio $c_i^{\rm DMD}$ for each mode obtained by Delay-DMD are shown in

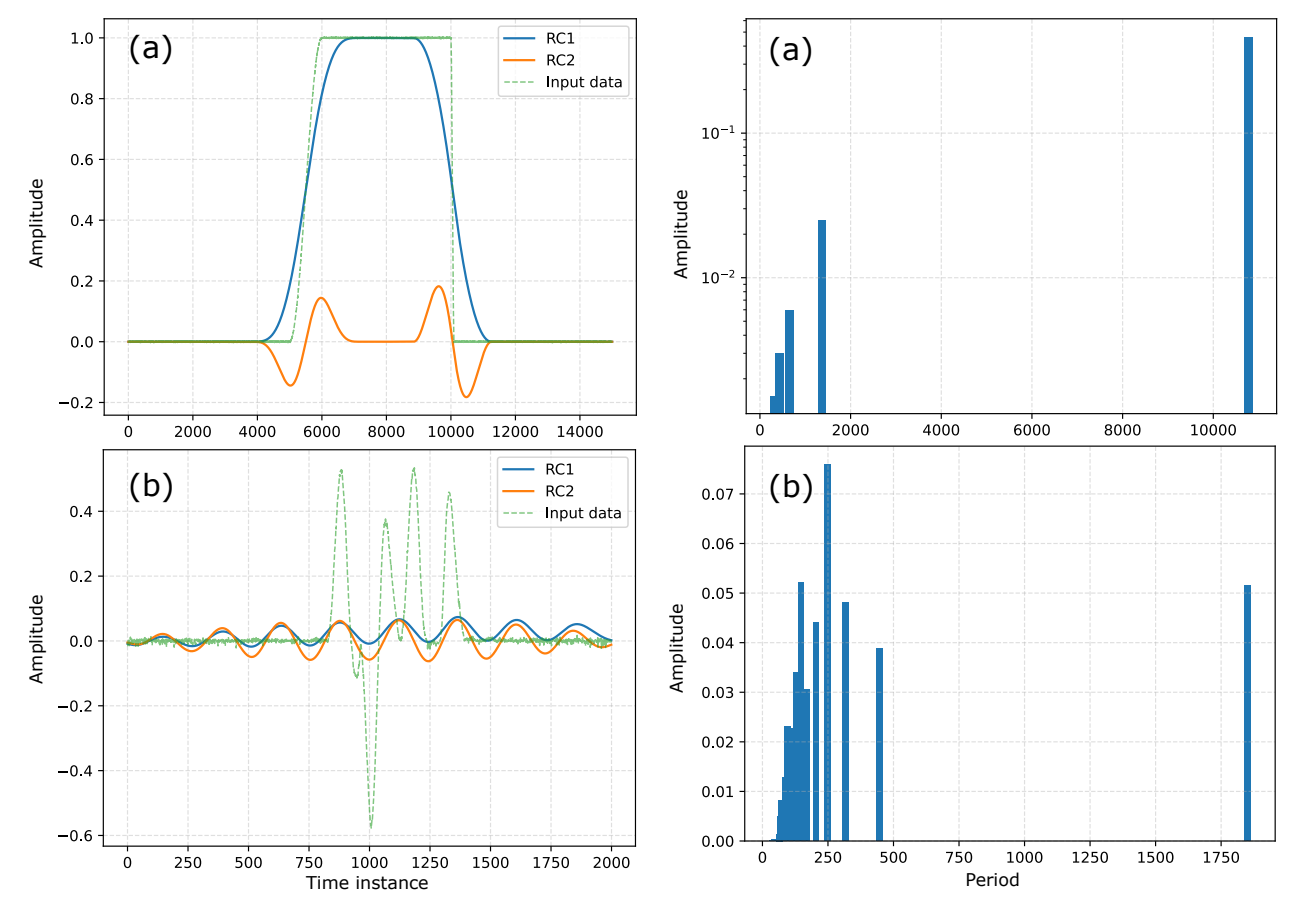


Fig. 8. SSA results for (a) toy model data and (b) turret punch data. The blue and orange lines show reconstructed signals $RC_1[n]$ and $RC_2[n]$, respectively. The dashed green line shows the input data (toy model or turret punch).

Fig. 9. DMD results for (a) toy model data and (b) turret punch data: period $T_i^{\rm DMD}$ versus contribution ratio $c_i^{\rm DMD}$ for each model.

Fig. 9(a) for the toy model and Fig. 9(b) for the turret punch data.

In Fig. 9(a), most DMD modes have real (non-oscillatory) eigenvalues; therefore, only five pairs of complex-conjugate modes are plotted. The contribution ratio $c_i^{\rm DMD}$ takes the largest value at $T_i^{\rm DMD}=10770.77,$ which corresponds to the total data length N=12000. The second dominant scale, $T_i^{\rm DMD}=1369.24,$ might correspond to $\tau_0=1000$ of the first half-sine segment in the toy model data. The smallest $T_i^{\rm DMD}$ among the oscillatory modes is 323.63, which is significantly larger than $\tau_1=100.$ This indicates that Delay-DMD fails to isolate short-lived transient segments in the toy model.

In Fig. 9(b), the contribution ratio $c_i^{\rm DMD}$ takes the largest value at $T_i^{\rm DMD}=1852.31$, which corresponds to the total data length N=2000. The second-largest $T_i^{\rm DMD}$ is 445.63, which is smaller than the distance

 $L_{0,8}$ between the locations L_0 and L_8 . This suggests that Delay-DMD does not recover the overall pulsive pattern spanning L_0 to L_8 . Moreover, for $T_i^{\rm DMD} < 200$, the spectrum exhibits no significant peaks, implying that Delay-DMD fails to distinguish short-term rising or falling segments contained in the pulsive oscillation of the turret punch data.

5.3 Comparative discussion

The comparative analysis highlights fundamental limitations of the Hankel-based baselines in the present setting. SSA, although effective for decomposing long signals into oscillatory components, lacks a principled, unified way to quantify the time scale of each reconstructed component. As shown in Sec. 5.2, SSA tends to reproduce the original signal in the leading component and to generate residual sinusoidal artifacts in subsequent ones. Such decompositions fail to capture localized one-

shot pulsive events in both the toy model and the turret data.

Delay-DMD, on the other hand, explicitly assigns oscillatory time scales via eigen-analysis. However, the contribution spectra in Fig. 9 show that the dominant modes correspond either to the full data length or to broad oscillatory envelopes. Short transient scales—such as the falling segment of the toy waveform or localized rises in the turret sequence—are not represented by single modes; multiple oscillatory modes must be combined to approximate such non-stationary structures, which undermines physical interpretability.

In contrast, the proposed DEF method is explicitly designed to isolate one-shot pulsive structures. By aligning the embedding with the event length d^* , DEF directly captures the dominant transient scales without requiring repeated instances or stationary oscillations. Across both datasets, DEF identifies the correct pulsive scales where SSA fails to separate and Delay-DMD oversmooths. This capability is particularly valuable in industrial anomaly detection scenarios, where available data consist of sparse, one-shot transients rather than long stationary time series.

Overall, while SSA and Delay-DMD are useful generic Hankel-based decompositions, they do not, by construction, target non-repeating pulsive patterns. DEF provides a compact and interpretable representation of such dynamics and, in the present experiments, uniquely recovers the dominant pulsive time scales that align with the empirical structures reported in Sec. 3 and Sec. 4.

6 CONCLUSIONS

In this paper, we presented an alternative approach to analyzing temporal patterns by focusing on their duration. We studied time-series data $\{y(t)\}$ that resulted from a state space system controlled by a piecewise constant control input u(t). By identifying a linear dynamical model of subsequences (delay coordinates) and assuming that its discrete spectrum can describe the target signal y(t), we developed a framework called Data-driven Exponential Framing (DEF). DEF allows us to capture exponential decay rates associated with dominant temporal patterns based on the eigen-decomposition of the identified model. We demonstrated that DEF can identify two distinct lengths (or timescales) of subsequences in numerical data obtained from a harmonic oscillator-based model. We also applied DEF to pulsive current data collected from a turret punch and showed that the timescales derived by DEF can explain any combination of fundamental curves of the data. Futhermore, comparative analysis with SSA and DMD clearly shows the uniqueness of DEF as a compact and interpretable representation nonrepeating pulsive patterns. Therefore, we argue that DEF can characterize temporal patterns inherent in time series data by their duration (timescales).

DEF can be applied to a wide range of data that can be described by their discrete spectrum, as it requires only the two design parameters (L and σ^2) and does not require any prior information on the systems. While our main experiments considered piecewise constant exogenous signals, the formulation naturally generalizes by augmenting input lags in the delay vector when inputs exhibit intra-plateau dynamics (see Appendix A), preserving the same estimation pipeline. In addition, the framework is not restricted to single-output settings; extending it to multi-output problems is straightforward and may further broaden its applicability.

Finally, we emphasize the practicality of DEF. It enables extract fundamental temporal patterns from data, which can be reused as search queries to explore larger datasets. For system modeling and control, the bases \boldsymbol{V}_i of DEF compactly represent pulse-driven dynamics, providing an efficient means for dimensionality reduction. Beyond these points, the DEF outputs serve directly in downstream analysis and design: (i) as pattern-level descriptors that validate physics-based models by comparing predicted versus observed time scales; (ii) as compact targets for controller tuning and setpoint scheduling, where desired temporal responses (rise/fall durations) are specified and checked against $\{T_i\}$ and $\{A_{i,d^*}[n]\}$; and (iii) as search/indexing keys to retrieve similar episodes across different runs, lots, or machines. Importantly, DEF is complementary to known physics in manufacturing: it provides a data-grounded summary of dominant pulselike phenomena without requiring a full parametric model a priori, while still constraining and informing such models by exposing the critical timescales that must be reproduced.

ACKNOWLEDGEMENTS

The authors appreciate Mr. Yoshinori Mochizuki, Mr. Ippei Takasawa, Mr. Takuma Nishimura, Mr. Atsushi Otake, and Dr. Kenta Deguchi (Hitachi, Ltd.) for valuable discussion and provision of the measurement data.

REFERENCES

- [1] Scafetta, N., and Grigolini, P., 2002, "Scaling detection in time series: Diffusion entropy analysis," *Physical Review E*, **66**(3), p. 036130.
- [2] Leo, F., Hansson, T., Ricciardi, I., De Rosa, M., Coen, S., Wabnitz, S., and Erkintalo, M., 2016,

- "Walk-off-induced modulation instability, temporal pattern formation, and frequency comb generation in cavity-enhanced second-harmonic generation," *Physical Review Letters*, **116**(3), p. 033901.
- [3] Keogh, E., Lin, J., Fu, A. W., and Van Herle, H., 2006, "Finding unusual medical timeseries subsequences: Algorithms and applications," *IEEE Transactions on Information Technology in Biomedicine*, **10**(3), pp. 429–439.
- [4] Gugulothu, N., TV, V., Malhotra, P., Vig, L., Agarwal, P., and Shrof, G., 2018, "Predicting remaining useful life using time series embeddings based on recurrent neural networks," *International Journal of Prognostics and Health Management*, **9**(1), pp. 1–13.
- [5] Fu, T. C., Chung, F. L., Ng, V., and Luk, R., 2001, "Evolutionary segmentation of financial time series into subsequences," In Proceedings of the IEEE Conference on Evolutionary Computation, Vol. 1, pp. 426–430.
- [6] Lovrić, M., Milanović, M., and Stamenković, M., 2014, "Algoritmic methods for segmentation of time series: An overview," *Journal of Contemporary Economic and Business Issues*, 1(1), pp. 31–53.
- [7] Takatsugi, S., Uchiyama, T., Murayama, J., Ishikuro, T., Fujioka, O., and Ohmori, A., 2017, "Development of operation detection system of check ring in injection molding machine," *Journal of the Japan Society for Precision Engineering*, **83**(3), pp. 281–286 in Japanese.
- [8] Takahashi, Y., Masuda, A., Iduka, T., and Sone, A., 2013, "Condition monitoring of the turret punch press using wavelet transformation," In Proceedings of the 12th symposium on evaluation and diagnosis, pp. 62–65 in Japanese.
- [9] Terada, M., Minakawa, T., Anzai, H., and Imamura, M., 2021, "Unsupervised discovery of repetitive activity patterns in acceleration time series data," *IEEJ Transactions on Electronics, Information and Sys*tems, 141(9), sep, pp. 1039–1047 in Japanese.
- [10] Kono, Y., Tajima, Y., and Mochizuki, Y., 2022, "A dynamical approach to determining time window for time-series anomaly detection," In 2022 IEEJ Annual Conference on Electronics, Information and Systems, pp. 22–25 in Japanese.
- [11] Ulsoy, A. G., and Koren, Y., 1993, "Control of machining processes," *Journal of Dynamic Systems, Measurement and Control, Transactions of the ASME*, **115**(2B), pp. 301–308.
- [12] Esling, P., and Agon, C., 2012, "Time-series data mining," *ACM Computing Surveys*, **45**(1), pp. 1–34.
- [13] Lin, J., Keogh, E., Lonardi, S., and Patel, P., 2002,

- "Finding motifs in time series," In Proceedings of the 2nd Workshop on Temporal Data Mining, pp. 53–68.
- [14] Lam, H. T., Pham, N. D., and Calders, T., 2011, "Online discovery of top-k similar motifs in time series data," In Proceedings of the 11th SIAM International Conference on Data Mining (SDM2011), pp. 1004–1015.
- [15] Imamura, M., and Nakamura, T., 2021, "Spikelet: An adaptive symbolic approximation for finding higher-level structure in time series," In Proceedings of 2021 IEEE International Conference on Data Mining (ICDM), pp. 1120–1125.
- [16] Keogh, E., Lin, J., and Fu, A., 2005, "HOT SAX: Efficiently finding the most unusual time series subsequence," In Proceedings of Fifth IEEE International Conference on Data Mining (ICDM'05), pp. 8–15.
- [17] Mueen, A., and Keogh, E., 2010, "Online discovery and maintenance of time series motifs," In Proceedings of the ACM SIGKDD International Conference on Knowledge Discovery and Data Mining, pp. 1089–1098.
- [18] Imamura, M., and Nakamura, T., 2015, "Window size dependency on anomaly detection based on discord for time series," *IEEJ Transactions on Electronics, Information and Systems*, 135(10), pp. 1244–1254.
- [19] Ye, L., and Keogh, E., 2009, "Time series shapelets: A new primitive for data mining," In Proceedings of the ACM SIGKDD International Conference on Knowledge Discovery and Data Mining, pp. 947– 955.
- [20] Yamaguchi, A., and Nishikawa, T., 2019, "Oneclass learning time-series shapelets," In Proceedings of 2018 IEEE International Conference on Big Data (Big Data 2018), pp. 2365–2372.
- [21] Yamaguchi, A., Maya, S., Maruchi, K., and Ueno, K., 2020, "LTSpAUC: Learning time-series shapelets for partial AUC maximization," *Big Data*, **8**(5), pp. 391–411.
- [22] Takens, F., 1981, "Detecting strange attractors in turbulence," In *Lecture Notes in Mathematics*, Vol. 898. Springer-Verlag, pp. 366–381.
- [23] Abarbanel, H. D. I., Carroll, T. A., Pecora, L. M., Sidorowich, J. J., and Tsimring, L. S., 1994, "Predicting physical variables in time-delay embedding," *Physical Review E*, 49(3), pp. 1840–1853.
- [24] Tan, E., Algar, S., Corrêa, D., Small, M., Stemler, T., and Walker, D., 2023, "Selecting embedding delays: An overview of embedding techniques and a new method using persistent homology," *Chaos*,

- **33**(3), pp. 1–35.
- [25] Hassani, H., 2007, "Singular spectrum analysis: Methodology and comparison," *Journal of Data Science*, **5**(2), pp. 239–257.
- [26] Le Clainche, S., and Vega, J. M., 2017, "Higher order dynamic mode decomposition," *SIAM Journal on Applied Dynamical Systems*, **16**(2), pp. 882–925.
- [27] Brunton, S. L., Brunton, B. W., Proctor, J. L., Kaiser, E., and Nathan Kutz, J., 2017, "Chaos as an intermittently forced linear system," *Nature Communications*, **8**(1), pp. 1–8.
- [28] Kono, Y., and Tajima, Y., 2025, "Data-driven exponential framing for one-shot pulsive temporal patterns," In Proceedings of 2025 IFAC Modeling, Estimation and Control Conference, p. 1070.
- [29] Golyandina, N., Nekrutkin, V., and Zhigljavsky, A. A., 2001, *Analysis of time series structure: SSA and related techniques* CRC press.
- [30] Schmid, P. J., 2010, "Dynamic mode decomposition of numerical and experimental data," *Journal of fluid mechanics*, **656**, pp. 5–28.
- [31] Phan, M. Q., Lim, R. K., and Longman, R. W., 1998, Unifying input-output and state-space perspectives of predictive control Technical Report 3044, Department of Mechanical and Aerospace Engineering, Princeton University, Princeton, NJ.
- [32] Pan, S., and Duraisamy, K., 2020, "On the structure of time-delay embedding in linear models of non-linear dynamical systems," *Chaos: An Inter-disciplinary Journal of Nonlinear Science*, **30**(7), p. 073135.
- [33] Akaike, H., 1973, "Information theory and an extension of the maximum likelihood principle," In Proceedings of the 2nd International Symposium on Information Theory, B. N. Petrov and F. Caski, eds., pp. 267–281.
- [34] Hastie, T., Tibshirani, R., and Friedman, J., 2009, The Elements of Statistical Learning Data Mining, Inference, and Prediction Springer.

APPENDIX A: RELAXATION OF THE PIECEWISE-CONSTANT INPUT ASSUMPTION

In Sec. 2 we introduced DEF under the assumption that the exogenous input $\boldsymbol{u}(t)$ is piecewise constant (PWC). Here, we relax this restriction by augmenting the delay coordinates with input lags, thereby extending the formulation to general forced systems without altering the overall pipeline.

Consider extending Eq. (3) to incorporate input lags:

$$\frac{\mathrm{d}\boldsymbol{x}_d(t)}{\mathrm{d}t} = \left[\mathsf{A}_d, \mathsf{B}_d\right] \begin{bmatrix} \boldsymbol{x}_d(t) \\ \boldsymbol{u}_d(t) \end{bmatrix},\tag{28}$$

where $B_d \in \mathbb{R}^{d \times dm}$ and $u_d(t) \in \mathbb{R}^{dm}$ denotes the delay-coordinate vector of the input with sampling interval Δt :

$$\mathbf{u}_{d}(t) = \begin{bmatrix} \mathbf{u}(t) \\ \mathbf{u}(t - \Delta t) \\ \vdots \\ \mathbf{u}(t - (d - 1)\Delta t) \end{bmatrix}.$$
(29)

Including input delays provides a practical embedding for driven or controlled systems. For the PWC case treated in Sec. 2, the term $\mathsf{B}_d u_d(t)$ becomes constant within each plateau and is absorbed into the intercept, leaving the identified A_d unchanged. Thus, Eq. (28) can be viewed as a natural extension of the state equation in Sec. 2.

Once A_d and B_d are identified from data, the DEF decomposition extends in a straightforward way. For instance, the 1-step prediction becomes

$$\mathbf{x}_{d}(t_{0} + \Delta t) - \mathsf{B}_{d}\mathbf{u}_{d}(t_{0}) = \exp(\mathsf{A}_{d}\Delta t)\,\mathbf{x}_{d}(t_{0})$$

$$= \sum_{i=1}^{d} a_{i,d}(t_{0})\,\exp(\lambda_{i}\Delta t)\,\mathbf{V}_{i},$$
(30)

which is the forced analogue of Eq. (6). Accordingly, the subsequence expansion Eq. (8) is modified by subtracting the input contribution: for n = 0, 1, ..., d - 1,

$$y(t - (n-1)\Delta t) - b_{n,d}(t) \simeq \sum_{i=1}^{d} \tilde{a}_{i,d}(t) \exp(-\nu_i n \Delta t),$$
(31)

where $b_{n,d}(t)$ is the *n*-th component of $\mathsf{B}_d u_d(t)$. Thus, the amplitude estimation in Eq. (9) becomes

$$\tilde{a}_{i,d}(t) \simeq \sum_{n=0}^{d-1} (y(t - (n-1)\Delta t) - b_{n,d}(t)) \exp(\nu_i n \Delta t).$$
(32)

This adjustment shows that the input effect is explicitly removed prior to estimating $\tilde{a}_{i,d}(t)$.

In terms of system identification, both A_d and B_d are obtained by minimizing a modified regression error:

$$E_d = \left\| \mathsf{Y}_d^{(d,N)} - \tilde{\mathsf{A}}_d \mathsf{X}_d^{(d,N)} - \tilde{\mathsf{B}}_d \mathsf{U}_d^{(d,N)} \right\|_{\mathsf{F}}^2, \tag{33}$$

where $\mathsf{U}_d^{(M_1,M_2)}=[\boldsymbol{u}_d(M_1-1),\ldots,\boldsymbol{u}_d(M_2-2)].$ Similarly, the AIC criterion in Eq. (15) extends to

$$AIC(d) = \frac{\left\| \mathsf{Y}_{d}^{(d+L-1,N)} - \mathsf{C}_{d} \mathsf{Z}_{d,L} \right\|^{2}}{N - d - L} + \frac{2d}{N - d - L} \sigma^{2},$$
(34)

with

$$\mathsf{Z}_{d,L} := \tilde{\mathsf{A}}_{d}^{L} \mathsf{X}_{d}^{(d,N-L+1)} + \sum_{i=1}^{L} \tilde{\mathsf{A}}_{d}^{L-i} \tilde{\mathsf{B}}_{d} \, \mathsf{U}_{d}^{(d+i-1,N-L+i)}. \tag{35}$$

Finally, the amplitude at time n is evaluated as

$$\tilde{A}_{i,d^*}[n] = \left(\boldsymbol{x}_d[n+1] - \mathsf{B}_d \boldsymbol{u}_d[n]\right)^\top \tilde{\boldsymbol{V}}_i. \tag{36}$$

In summary, the extension above preserves the structure of the DEF pipeline presented in Sec. 2. The only difference is the explicit subtraction of the input contribution through the matrices B_d and U_d , while all subsequent steps (eigendecomposition, extraction of ν_i , and amplitude evaluation) remain identical. This guarantees that the methodology is not restricted to PWC inputs and can be seamlessly applied to general forced systems.

APPENDIX B: EFFECT OF THE HORIZON LENGTH L ON THE SHAPE OF THE INFORMATION CRITERION

To illustrate how the choice of horizon length L affects the information criterion, we compared three representative settings: L=1, L=5, and L=20. Since the absolute value of $\mathrm{AIC}(d)$ varies with L, we normalized each curve by subtracting its minimum value, i.e.,

$$AIC_{rel}(d; L) = AIC(d; L) - \min_{d} AIC(d; L),$$
 (37)

so that all curves are aligned at zero. This normalization allows us to compare the shape and the consistency of discriminative ability across different L.

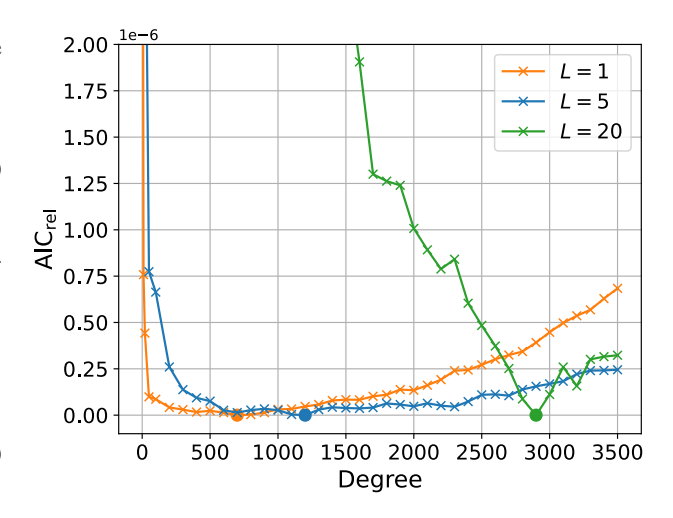


Fig. 10. $AIC_{rel}(d; L)$ for L = 1, 5, 20.

Figure 10 shows the $\mathrm{AIC}_{\mathrm{rel}}(d;L)$ curves for L=1, L=5, and L=20. For L=1, the curve is convex but exhibits a steep rise for larger d, which gives the appearance of a trivial or "already-known" solution. This reduces the practical informativeness of the criterion. For L=5, the curve is convex with a gradual rise, striking a good balance between discriminative sharpness and robustness across model orders. For L=20, the curve tends to slope downwards, becoming susceptible to noise accumulation, which undermines the reliability of model order comparison. These observations support our heuristic choice of L=5 in the main experiments, as it achieves a balance between consistency and discriminative effectiveness.

APPENDIX C: PEAK EXTRACTION ALGORITHM

For completeness, we provide here the definitions and explanations underlying Algorithm 2 (Peak extraction). Let \tilde{T}_i denote the estimated period corresponding to the i-th delay component, and let $\tilde{A}_{i,d^*}[n]$ be the associated amplitude spectrum at time index n with embedding order d^* . The goal is to extract dominant peaks in the $(\tilde{T}_i, \tilde{A}_{i,d^*})$ spectrum.

The scoring criterion combines two factors: (i) the peak prominence p_i , defined as the excess amplitude above a local baseline computed within a sliding window of log-period width w, and (ii) the isolation score s_i , which measures how well the candidate stands out relative to the local background energy e_i in its neighborhood. A small stabilizer ϵ is included to ensure numerical robustness when the background energy is close to zero.

Algorithm 2: Peak extraction on time-scale spectrum $(\tilde{T}_i, \tilde{A}_{i,d^*}[n])$ at a fixed time n

```
Input: Pairs \{(\tilde{T}_i, \tilde{A}_{i,d^*}[n])\}_{i=1}^{d^*} at a fixed n
     Output: Reported dominant peaks \mathcal{P}_{\mathrm{rep}}(n)
 1 \ a_i \leftarrow |\tilde{A}_{i,d^*}[n]|, \quad x_i \leftarrow \log \tilde{T}_i;
 2 Sort \{(x_i, a_i)\} in ascending x_i;
 b_i \leftarrow \text{running\_median}(a_i; w);
 4 p_i \leftarrow \max(0, a_i - b_i);
 \mathbf{5} \ \ \mathbf{for} \ i = 1 \ \mathbf{to} \ d^* \ \mathbf{do}
           \mathcal{N}_i \leftarrow \{ j \neq i \mid w/2 \leq |x_j - x_i| \leq w \};
       e_i \leftarrow \sqrt{\frac{1}{|\mathcal{N}_i|} \sum_{j \in \mathcal{N}_i} a_j^2};
s_i \leftarrow \frac{p_i}{\epsilon + e_i};
 9 q_i \leftarrow p_i \cdot s_i;
10 \mathcal{C} \leftarrow \emptyset;
11 for i=1 to d^* do
          if q_i is the maximum within
          \{j: |x_j - x_i| \le w\} then 
 \triangle Add (i, \tilde{T}_i, a_i, q_i) to C;
14 rank C by q_i (descending);
15 \mathcal{P}_{\text{all}}(n) \leftarrow \{ (i, \tilde{T}_i) \in \mathcal{C} \mid q_i \geq \theta \};
16 \mathcal{P}_{rep}(n) \leftarrow top\text{-}K entries of \mathcal{C} by q_i;
```

The final dominance score is given by $q_i = p_i \cdot s_i$, balancing absolute height with relative isolation. Peaks with q_i above a threshold Θ are considered significant, and among them, up to K top-ranked peaks are retained for reporting. These parameters (w, ϵ, Θ, K) were fixed at default values in our experiments, but can be tuned without altering the qualitative outcome.

This procedure corresponds to the heuristic visual identification employed in the main experiments, while the algorithm provides a reproducible formalization of the same criterion.